A STUDY OF NON-GRAVITATIONAL EFFECTS OF COMET C/1995 O1 HALE–BOPP

SŁAWOMIRA SZUTOWICZ[1,⋆], MAŁGORZATA KRÓLIKOWSKA[1] and GRZEGORZ SITARSKI[1,2]

[1]*Space Research Centre of Polish Academy of Sciences, Bartycka 18A, 00–716, Warsaw, Poland;*
[2]*Institute of Theoretical Physics, University in Bialystok, Lipowa 41, 15-424 Białystok, Poland*

(Received 28 February 2002; Accepted 16 July 2002)

Abstract. The role of non-gravitational forces in the evolution of orbital motion of C/1995 O1 (Hale–Bopp) has been investigated. In orbital calculations the observational material covering the period from April 1993 up to August 2001 was used. To model the non-gravitational acceleration, observed and theoretical profiles of the H_2O production rates were employed. A set of forced precession models of a rotating cometary nucleus consistent with the observed spin axis orientation was fitted to positional observations. The non-gravitational models allowed us to constrain the mass and radius of the comet. The orbital evolution of Comet Hale–Bopp was investigated over ±400 k y using two sets of randomly varied orbital elements well representing all positional observations in the pure gravitational case, as well as in the non-gravitational case. The calculations showed that the comet's motion is predictable only over an interval of a few orbital periods. The statistical conclusions change significantly when non-gravitational effects are included in the analysis.

Keywords: Comet Hale–Bopp, long-period comet, non-gravitational effects

1. Introduction

C/1995 O1 (Hale–Bopp) has provided an unprecedented opportunity to follow the evolution of activity and orbital motion of a long-period comet over a very large range of heliocentric distances. The comet was discovered on 23 July 1995 at 7 AU from the Sun in a state of major activity. The observed high water production rates indicate that non-gravitational activity should influence the orbital motion of the comet.

2. Heliocentric Dependence of Production Rates

As comets approach the Sun, the solar radiation heats the surface layers of their nuclei and induces sublimation of molecular ices. At large heliocentric distances the activity is driven by sublimation of carbon monoxide, whereas sublimation of water ice from the surface layer becomes efficient at about 3 AU from the Sun. To

⋆ E-mail: slawka@cbk.waw.pl

Earth, Moon and Planets **90:** 119–130, 2002.
© 2002 *Kluwer Academic Publishers. Printed in the Netherlands.*

analyze the profile of activity of Comet Hale–Bopp, 104 measurements of the water production rates made between 7 April 1996 and 29 December 1997 were used. Several groups observed the comet over a very broad spectral range from ultraviolet to infrared. Figure 1 shows the variation of observed water outgassing rates versus heliocentric distance. Different symbols denote observations as they were given by the authors with the exception of the measurements of the OH radical, which were converted to the water production rate ($Q_{H_2O} = Q_{OH}/0.856$). The curves and lines represent theoretical sublimation rates and profiles of the water release rate fitted to the observations.

The general form of the water sublimation rate as a function of the heliocentric distance, r(AU), can be written as:

$$Q_{H_2O}(r) = Q_m \cdot g^*(r).$$

The values of the constant Q_m(mol./s) for the profiles studied are given in Table I. For the dimensionless function $g^*(r)$ two types of expressions are proposed:

$$g^*(r) = \alpha \left(\frac{r}{r_o}\right)^{-m} \left[1 + \left(\frac{r}{r_o}\right)^{n}\right]^{-k} \quad \text{or} \quad g^*(r) = h(r) = r^{-n}.$$

The power law r^{-n} was used to fit the pre- and post- perihelion observations separately by least-squares to $Q_m \cdot h(r)$ (see Table I). The former expression $g^*(r)$ stands for one of the functions: $g(r)$, $g'(r)$ or $f(r)$ which are representative in the following three cases:

- Water sublimation rate for an isothermal cometary nucleus. Then $g^*(r) = g(r)$, where the function $g(r)$ is commonly used in orbital calculations for non-gravitational effects.
- Outgassing restricted to subsolar point only. Then $g^*(r) = g'(r)$ and the appropriate coefficients for the function $g'(r)$ are taken from
- Water sublimation rate as observed for Comet Hale–Bopp. In this case $g^*(r) = f(r)$ and the production rates are fitted by least-squares to the expression $Q_m \cdot f(r)$.

The values of exponents: n, m, k, the scale distance r_o and the coefficient α for all mentioned functions are listed in Table I.

3. Non-Gravitational Models

In orbital studies the widely used form of the non-gravitational acceleration is (Marsden et al., 1973):

$$a_i = A_i \cdot g^*(r), \quad i = 1, 2, 3,$$

where a_i represent the radial, transverse and normal components, respectively. Hereafter the expression $g^*(r)$ will signify one of the functions $g(r)$, $f(r)$ or $h(r)$.

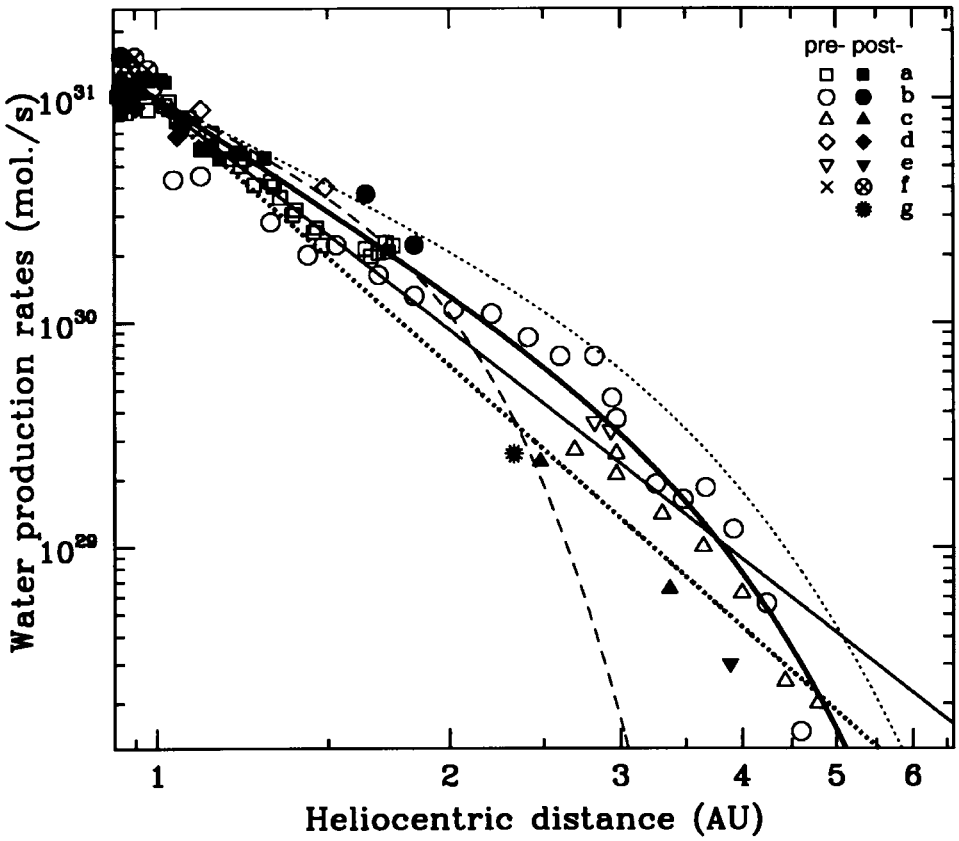

Figure 1. Heliocentric variation in the production rates of water. The open and filled symbols represent measurements performed before and after perihelion passage, respectively. (a) SWAN observation of Lyman-α (Combi et al., 2000). (b) Observation of OH at Nancay (Colom et al., 1997; Biver et al., 1997). (c) IUE and Hubble Space Telescope (Weaver et al., 1999). (d) IR observations (Dello Russo et al., 2000). (e) Infrared Space Observatory (Crovisier et al., 1999). (f) OH observations in UV, SOLSTICE (Woods et al., 2000). (g) Southwest Ultraviolet Imaging System (Stern et al., 1999). The dotted curve shows the theoretical sublimation rate at subsolar point ($Q_m \cdot g'(r)$), and the dashed one is the surface-averaged sublimation of an isothermal nucleus ($Q_m \cdot g(r)$). The solid curve is a least-squares fit of all observations to the function $Q_m \cdot f(r)$. The solid and dotted straight lines are results of fitting to a power law the pre- and post-perihelion observations, respectively.

The above mentioned standard model can be written as:

$$a_i = A \cdot g^*(r) \cdot C_i(\eta, I, \phi + \vartheta(t)), \quad i = 1, 2, 3,$$

where the direction cosines C_i of the non-gravitational acceleration depend on: the obliquity of the orbit plane to the nucleus equator, I, the solar longitude at perihelion, ϕ, the true anomaly, $\vartheta(t)$, of a comet and the lag angle, η, of the maximum outgassing behind the subsolar meridian.

Another type of the non-gravitational model is the model of forced precession of the spin axis of cometary nucleus proposed by Whipple and Sekanina (1979).

TABLE I

$g^*(r)$	α	m	n	k	r_o(AU)	Q_m(mol./s)
$g(r)$	0.111262	2.150	5.093	4.6142	2.808	$1.11 \cdot 10^{30}$
$g'(r)$	0.002726	2.100	3.200	3.9200	5.600	$1.11 \cdot 10^{30}$
$f(r)$	0.008860	2.828	3.761	3.7440	5.331	$7.8995 \cdot 10^{28} \pm 425$
		± 0.332	± 4.459	± 25.082	± 12.251	
$h(r)$	Pre-perihelion		$n = 3.39 \pm 0.08$			$9.732 \cdot 10^{30} \pm 1.061$
	Post-perihelion		3.87 ± 0.15			$9.407 \cdot 10^{30} \pm 1.063$

According to this model, nonlinear variations of the direction of the spin axis with time are caused by changes in the reaction force acting on the non-spherical nucleus. The orbital components of the non-gravitational acceleration are functions of time:

$$a_i = A \cdot f(r) \cdot C_i(\eta, I(t), \phi(t) + \vartheta(t)), \quad I = 1, 2, 3.$$

The parameters of the model are: A, η, I, ϕ, s and f_p. The last two parameters: the nucleus oblateness, $s = 1 - R_b/R_a$, and precessional factor, f_p, are hidden in the time dependences of the angles I and ϕ. They are related to the equatorial radius, R_a, of the nucleus and to its rotation period, P_r, by the expression: $\frac{P_r}{R_a} = \frac{4\pi f_p}{5s}$.

The parameters of all mentioned models were determined along with the six orbital elements $(T, q, e, \omega, \Omega, i)$ in an iterative process of orbit improvement.

4. Orbital Calculations and Results

The orbital motion of C/1995 O1 (Hale–Bopp) was investigated based on 3533 astrometric observations made between 1993 April 27 and 2001 August 13. The observations used were selected according to an objective data selection procedure (Bielicki and Sitarski, 1991). The pure gravitational orbit fits to the observations give an RMS of 1.″28. However, the orbital solutions influenced by the non-gravitational effects give a better fit to the observations of the comet, with a mean residual 1.″07 and 1.″06 for the models: $A_i \cdot g^*(r)$ and $A \cdot g^*(r) \cdot C_i$, respectively. The orbital elements and the non-gravitational parameters are listed in Table IV and Table II.

The non-gravitational acceleration can be discussed in terms of some of the physical parameters of the cometary nucleus. The values of the parameter A de-

TABLE II

Non-gravitational parameters obtained from the orbital solution for two types of models: $a_i = A_i \cdot g^*(r)$ and $a_i = A \cdot g^*(r) \cdot C_i(\eta, I, \phi + \vartheta)$, where $g^*(r)$ represents functions: $g(r)$, $f(r)$ or $h(r)$ (Epoch: 1993 April 3.0 E.T.). The nucleus mass M was estimated based on appropriate values of the parameter A

	$A_i \cdot g(r)$	$A_i \cdot f(r)$	$A_i \cdot h(r)$
A_1 (10^{-8} AU/day^2)	1.5224 ± 0.0316	1.5678 ± 0.0331	1.5384 ± 0.0319
A_2 (10^{-8} AU/day^2)	0.1214 ± 0.0054	0.1248 ± 0.0057	0.1278 ± 0.0057
A_3 (10^{-8} AU/day^2)	-0.0191 ± 0.0118	-0.0206 ± 0.0121	-0.0208 ± 0.0126
Mean residual	1.″07	1.″07	1.″06
	$A \cdot g(r) \cdot C_i$	$A \cdot f(r) \cdot C_i$	$A \cdot h(r) \cdot C_i$
A (10^{-8} AU/day^2)	1.5085 ± 0.0311	1.5521 ± 0.0322	1.5209 ± 0.0311
η (deg)	8.16 ± 0.61	7.82 ± 0.51	8.94 ± 0.62
I_o (deg)	55.25 ± 3.05	53.50 ± 2.75	57.02 ± 2.65
ϕ_o (deg)	80.71 ± 5.49	88.05 ± 5.8	85.88 ± 4.90
Mean residual	1.″06	1.″06	1.″06
M (10^{14} kg)	2.466	2.142	2.346

rived from orbit determinations for models $A \cdot g^*(r) \cdot C_i$ were used to calculate the nucleus' mass, M (see Table II) from:

$$M = \frac{m v Q_m}{A \alpha},$$

where m is the molecular mass of water and v is the average ejection speed of the molecules. Putting $v = 0.16 + 0.1q$ km/s as a function of perihelion distance q(AU) (Rickman et al., 1987), one would estimate $v = 0.25$ km/s for Comet Hale–Bopp. The radius of an ice sphere of mass $M \approx 2.3 \cdot 10^{14}$ kg and of density $0.1 \cdot 10^{12} \leq \rho \leq 1.0 \cdot 10^{12}$ kg/km^3 is $8.2 \leq R_{min} \leq 3.8$ km. This is about a factor of 4 to 5 less than the best estimate of the radius for Comet Hale–Bopp. However, the comet's nucleus is not active over its entire surface and the contribution of sublimation from the grain halo surrounding the nucleus is unknown. Assuming the radius of the nucleus as equal to 20 km and taking into account the above mentioned limits for an ice sphere, one would expect that the activity level, f_a, of the comet is $17\% \leq f_a \leq 4\%$.

It was impossible to determine f_p and s along with the other parameters of the forced precession model. To derive reasonable values for all 12 parameters of the model a longer time span of observations is needed. Thus we calculated a set of values for the precessional factor, f_p, and oblateness, s, for a cometary nucleus of the radius between 10 km to 35 km (Weaver and Lamy, 1997) with the

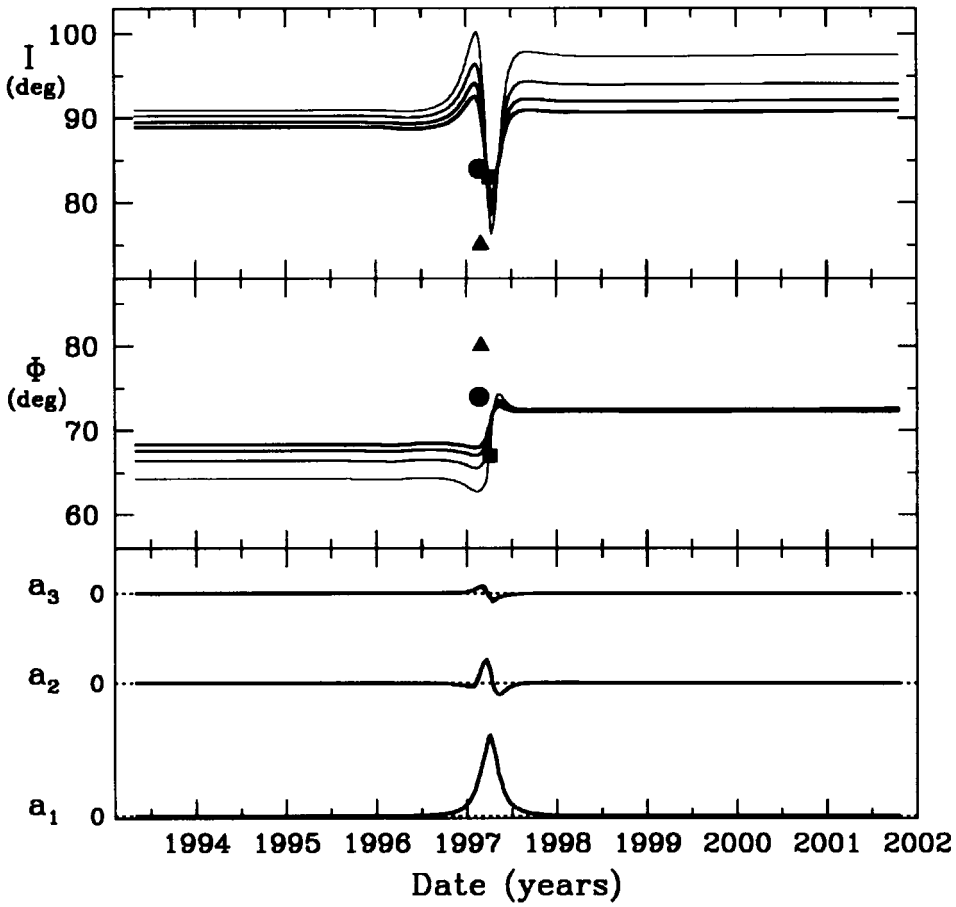

Figure 2. Time variation of the equatorial obliquity of nucleus, I, the solar longitude at perihelion, ϕ, and orbital components of the non-gravitational acceleration a_i derived from the forced precession model. The water outgassing from the comet nucleus was approximated by a function $Q_m \cdot f(r)$ (see Table I). An elongated nucleus ($s = -0.3$) with the rotation period $P_r = 11.34$ h was assumed. The curves from the thinnest to the thickest correspond to values of the nucleus radius as follows: 15 km, 20 km, 25 km and 30 km. Filled symbols denote the position of spin axis derived from observations of the arcs jets: square (Jorda et al., 1997), circle (Licardo et al., 1997) and triangle (Sekanina, 1998).

rotation period $P_r = 11.34$ hours (Jordan et al., 1997). Orbital calculations showed that precession models best fit the positional observations if the radius is larger than 15 km and the oblateness of the nucleus falls within the range from -0.3 to -0.5. The precession parameters derived for a nucleus of radius 20 km are shown in Table III. The changes of the spin axis orientation and the components of the non-gravitational acceleration due to forced precession are shown in Figure 2 for the models with a nucleus of different sizes ($15 \leq R \leq 30$ km) but the same oblateness ($s = -0.3$). The series of image sequences of the arc structures from February through May 1997 allowed the orientation of the spin axis to be obtained

TABLE III

Non-gravitational parameters derived from a forced precession model: $a_i = A \cdot f(r) \cdot C_i(\eta, I(t), \phi(t) + \vartheta(t))$. All orbital solutions fit to observations with an RMS of 1.″06 (Epoch: 2001 Oct.18.0 E.T.). The parameters f_p and s were assumed to be fixed and calculated for a nucleus of radius 20 km, rotating with the period 11.34 h

A 10^{-8} AU/day^2	η deg	I_o deg	Φ_o deg	f_p (10^5 AU/day)	s
1.4281 ± 0.0335	7.44 ± 0.88	89.89 ± 1.40	70.09 ± 1.51	-0.42187	-0.3
1.3617 ± 0.0263	8.16 ± 0.94	94.10 ± 1.22	72.52 ± 1.24	-0.56249	-0.4
1.3112 ± 0.0275	8.98 ± 1.02	97.45 ± 1.14	73.92 ± 1.16	-0.70311	-0.5

in equatorial coordinates. These data were recalculated to I and ϕ and are shown in Figure 2 with different symbols.

5. Dynamical Evolution

The long-term orbital evolution of Comet Hale–Bopp was calculated by Bailey et al. (1996). As the starting set of possible trajectories they took an ensemble of a few dozen heliocentric orbits for an epoch near the 1997 perihelion passage, derived from various arcs of pre-perihelion observations. They found that "the ensemble half-life for the comet to be captured or ejected is of the order of 0.5 Myr, in the backwards integrations and 1.2 Myr in the forward integrations". The past and future motion of the comet was also discussed by Marsden (1997) on the basis of several orbit determinations, where the longest arc of observations included post-perihelion measurements up to the end of 1997.

Our sets of starting orbits for the integration of comet motion are constructed in a different way. Since we do not know the true orbit, we take a set of randomly selected orbits which all agree well with the observations used for the nominal orbit determination (for orbital elements of the nominal orbit see Table IV). According to Sitarski's procedure (1998), we randomly selected a set of 100 orbits well representing the positional observations. Thus we have a series of 101 current orbits in which the comet 'could' move. The ranges of randomly selected orbital parameters in the pure gravitational case and in the non-gravitational case are given in Table IV. These two sets of 101 orbits were evolved backwards and forwards up to 400 kyr. The equations of motion were numerically integrated in barycentric coordinates using the recurrent power series method (Sitarski, 1989) taking into account the perturbations by all nine planets. For the second set of orbits non-gravitational effects were included in the dynamical evolution. We assumed that non-gravitational accelerations accumulated over one period remain constant in

TABLE IV

Range of orbital elements around nominal orbit (Epoch: 1993 April 3.0 ET = JD2449080.5; Equinox: 2000.0) for randomly selected orbits in the pure gravitational case (set I) and in the non-gravitational case (set II). All 100 randomly selected orbits fit to 3533 positional observations (6931 equations) taken during the interval 1993 April 27 – 2001 August 13 with RMS of 1.″29 (set I) and 1.″07 (set II). Non-gravitational parameters A_1, A_2, A_3 are given in units of 10^{-8} AU/day^{-2}

Set I; pure gravitational case					
T	q	e	ω	Ω	i
19970401.63910	0.91811797	0.99652359	130.°40015	282.°43720	88.°98876
+0.00007	+0.00000070	+.00000056	+0.°00002	+0.°00002	+0.°00002
−0.00010	−0.00000054	−0.00000051	−0.°00002	−0.°00002	−0.°00002
Set II; non-gravitational case					
T	q	e	ω	Ω	i
19970401.63965	0.91806833	0.99648242	130.°40354	282.°43732	88.°98883
+0.00007	+0.00000215	+0.00000185	+0.°00018	+0.°00002	+0.°00004
−0.00009	−0.00000299	−0.00000185	−0.°00015	−0.°00001	−0.°00005
			A_1	A_2	A_3
			1.5224	0.1214	−0.01915
			+0.1208	+0.0136	+0.01785
			−0.0693	−0.0152	−0.03224

each revolution, even when a dramatic change in the orbit occurred. That implies that the non-gravitational parameters A_1, A_2, A_3 should be modified with the dynamical evolution of perihelion distance, q, and eccentricity, e. We obtained a simple function $\sim q^{2.78276} \cdot (1-e)^{-1.64026}$ for this modification. Without this assumption an unphysically high level of non-gravitational forces would be achieved when the orbital period or/and the perihelion distance decreases.

The results show all the possible types of dynamical evolution. The comet could be captured/ejected from the Oort cloud in the past/future 0.4 million years, or it could stay in a long-period orbit, or even experience a short-period stage, or a Sun-grazing transition. For example, the nominal orbit remained of long-period from the beginning to the end of integration, performing 210 revolutions around the Sun in the past and 62 in the future (the pure gravitational case). In the non-gravitational case the nominal orbit evolved quite differently. It experienced a short-period stage ($P < 200$ y) over 0.33 Myr in the past, and was ejected from the solar system after 0.32 Myr!

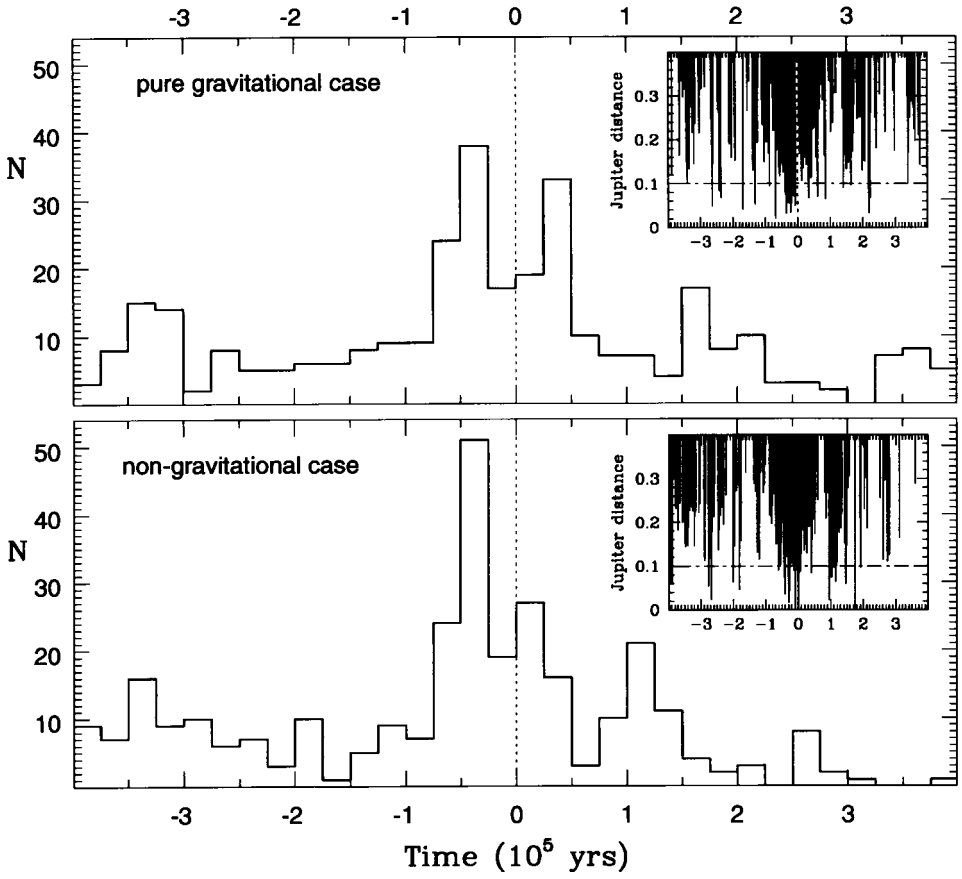

Figure 3. Distribution of all close approaches of the comet to Jupiter which appeared during the evolution of 101 orbits in the pure gravitational case and in the non-gravitational case, respectively. The evolution was performed backwards and forwards up to 400 kyr. The starting moment of integrations is shown by dotted vertical lines. The insets in both panels show the depths of all individual close encounters of the comet with Jupiter (closer than 0.33 AU).

The ascending node of the Comet Hale–Bopp's observed orbit (inclined almost perpendicular to the ecliptic) lies about 0.03 AU inside the orbit of Jupiter and thus the orbital evolution is dominated by Jovian perturbations. The distribution of all close comet encounters (closer than 0.33 AU) with Jupiter are shown in Figure 3 for pure gravitational and non-gravitational evolution. Some clustering of such encounters is visible in the past evolution up to 75 kyr, and a less significant clustering – in the future evolution up to 50 kyr.

The cumulative numbers of test objects from our sample captured in the past (or ejected in the future) over time-scales less than 50, 100, 200, 300, 400 kyr, respectively, are equal to 11 (10), 19 (17), 29 (28), 33 (34), 42 (36) for the pure gravitational evolution. The statistical results are different for non-gravitational integrations of a non-gravitational set of orbits. The corresponding cumulative

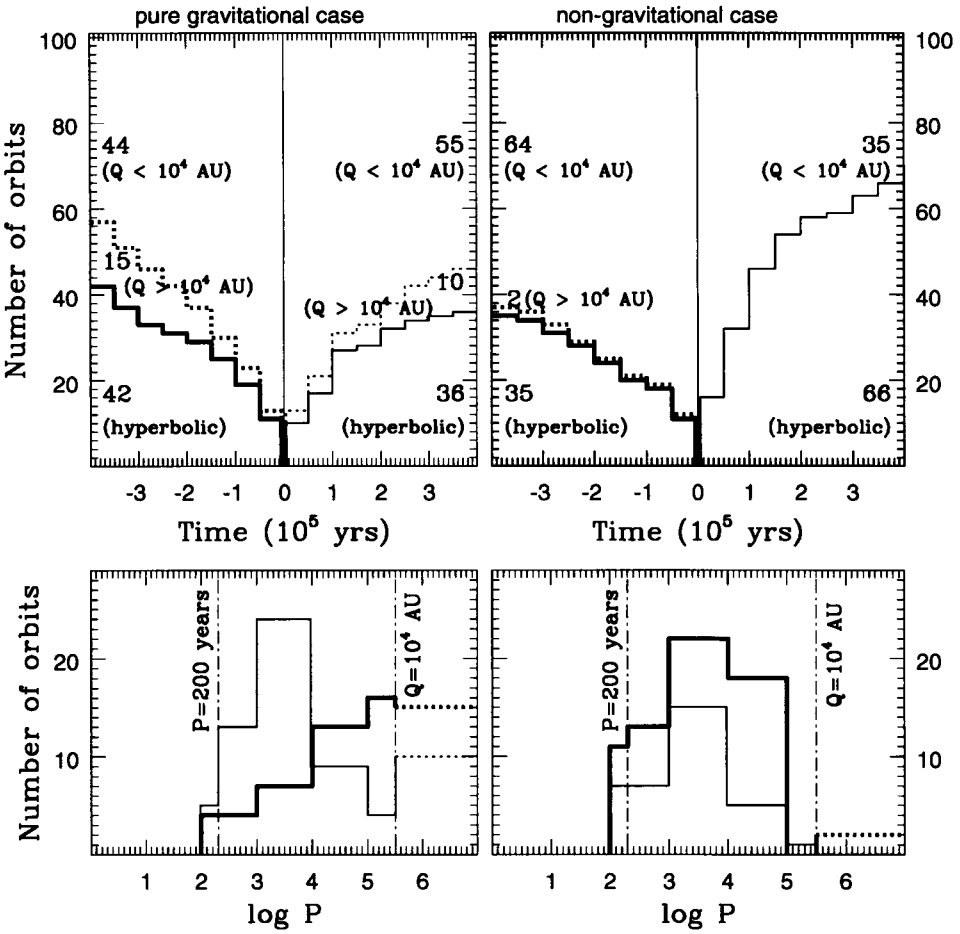

Figure 4. Upper panels: Cumulative number of orbits which evolved to: hyperbolic state (solid lines), long-period state with aphelion distance $Q \simeq 2a > 10^4$ AU (dashed lines) and $Q \simeq 2a < 10^4$ AU (rest of each sample), for the backwards (thick lines) and forwards integrations of 101 orbits up to 400 kyr. Lower panels: Number of orbits as a function of period for the past (thick lines) and the future subsets of orbits which evolved (after 400 kyr) to Halley state (20 y $< P <$ 200 y) or long-period state with $Q \simeq 2a < 10^4$ AU. Left side panels refer to pure gravitational evolution and right side panels show results for non-gravitational calculations.

numbers are then 11 (32), 18 (46), 28 (58), 34 (63), 35 (66) (see Figure 4). This suggests a larger ejection probability in the future than in the past (in contrast to Bailey et al. (1996) conclusion despite their longer integration intervals). We also found a few sungrazing orbits: 4 (8) in the past, and 3 (6) in the future for the pure gravitational case (non-gravitational case). This gives a similar probability of a sungrazing end-state of Hale–Bopp to Bailey et al. (1996) results (see their Table 7).

The mean number of past orbital revolutions is about four (six in the non-gravitational case) dozen for 42 (35) captured orbits, and a few hundred for the remaining 59 (76) orbits in the ensemble. Only one of 101 test particles in the non-gravitational case was captured just one revolution ago. Therefore it seems likely that Comet Hale–Bopp made several revolutions before coming to the inner part of the solar system.

6. Conclusions

- The orbital motion of C/1995 O1 (Hale–Bopp) evidently exhibits non-gravitational effects (compare the RMS in Table IV).
- The observed variations of water production rate with heliocentric distance do not follow the theoretical function $g(r)$ expected for an isothermal nucleus, but are very close to a model of outgassing restricted to the subsolar point on the nucleus surface (see Figure 1). That fact was previously pointed out by Weaver et al. (1999).
- The models of non-gravitational acceleration with various profiles of comet activity yield an estimate of the mass of the nucleus ($\approx 2.3 \cdot 10^{14}$ kg) and the lower limit of the radius (4–8 km). The presented forced precession models are consistent with the available observational data (see Figure 2) and indicate that the actual radius can be larger than 15 km.
- The evolutionary integrations show that the comet's motion is predictable only over a few orbital periods (less than 10 000 years). Non-gravitational effects play an essential role in the dynamical evolution of Comet Hale–Bopp. In particular, the non-gravitational future evolution gives a significantly higher probability of comet ejection from the Solar System than in the pure gravitational case (see Figure 4).

More advanced studies of the non-gravitational effects and the orbital evolution of Comet Hale–Bopp are in progress.

Acknowledgements

The authors would like to express their gratitude to Dr. Maciej Bzowski for his contributions to improve this paper. This work was supported by the Polish Committee for Scientific Research (the KBN grant 2.P03D.002.09).

References

Bailey, M. E., Emel'yanenko, V. V., Hahn, G. et al.: 1997, *M.N.R.A.S.* **281**, 916–924.
Bielicki, M. and Sitarski, G.: 1991, *Acta Astron.* **41**, 309–323.

Biver, N., Bockelée-Morvan, D., Colom, P., Crovisier, J., Germain B. et al.: 1997, *Earth Moon Planets* **78**, 5–11.
Colom, P., Gerard, E., Crovisier, J., Bockelée-Morvan, D., Biver, N., and Rauer, H.: 1997 *Earth Moon Planets* **78**, 37–43.
Combi, M. R., Reinard, A. A., Bertaux, J. L., and Quemerais, E.: 2000, *Icarus* **144**, 191–202.
Crovisier, J., Leech, K., Bockelée-Morvan, D., Lellouch, E. et al.: 1999, *ESA SP-427*, 137–140.
Dello Russo, N., Mumma, M. J., DiSanti, M. A. et al.: 2000, *Icarus* **143** 324–337.
Jorda, L., Rembor, K., Lecacheux, J., Colom, P., Colas, F., Frappa, E., and Lara, L. M.: 1997, *Earth Moon Planets* **77**, 167–180.
Licardo, J., Bellot Rubio, L. R., Casa, R., Gomez, A., Kidger, M. R., Sabalisk, N., Santos-Sanz, P. et al.: 1997, *Earth Moon Planets* **77**, 199–206.
Marsden, B. G.: 1997, *Earth Moon Planets* **79**, 3–15.
Marsden, B. G., Sekanina, Z., and Yeomans, D. K.: 1973, *Astron. J.* **78**, 211–225.
Rickman, H., Kamel, L., Festou, M. C., and Froeschle, Cl.: 1987, in *Diversity and Similarity of Comets*, ESA SP-278, 471–481.
Sekanina, Z.: 1988, *Astron. J.* **95**, 911–924.
Sekanina, Z.: 1998, *Astrophys. J.* **494**, L121–L124.
Sitarski, G.: 1989, *Acta Astron.* **39**, 345–349.
Sitarski, G.: 1998, *Acta Astron.* **48**, 547–561.
Stern, S. A., Colwell, W. B., Festou, M. C., Tamblyn, P. M., Parker, J. W., Slater, D. C., Weissman, P. R., and Paxton, L. J.: 1999, *Astron. J.* **118**, 1120–1125.
Weaver, H. A. and Lamy, P. L.: 1997, *Earth Moon Planets* **79**, 17–33.
Weaver, H. A., Feldman, P, D., A'Hearn, M. F., Arpigny, C., Brandt, J. C., and Stern, S. A.: 1999, *Icarus* **141**, 1–12.
Whipple, F. L. and Sekanina, Z.: 1979, *Astron. J.* **84**, 1894–1909.
Woods, T. N., Feldman, P. D., and Rottman, G. J.: 2000, *Icarus* **144**, 182–186.